PAPER

NJC
www.rsc.org/njc

# Effect of the calcination temperature of self-ordered mesoporous silicate on its adsorption characteristics for aromatic hydrocarbons

**Yuko Ueno,*[a] Tsutomu Horiuchi,[a] Akiyuki Tate,[a] Osamu Niwa,[a] Hao-shen Zhou,*[b] Takeo Yamada[b] and Itaru Honma[b]**

[a] *NTT Microsystem Integration Laboratories, 3-1 Morinosato Wakamiya, Atsugi, Kanagawa, 243-0198, Japan. E-mail: ueno@aecl.ntt.co.jp; Fax: +81-46-240-4728; Tel: +81-46-240-3549*

[b] *National Institute of Advanced Industrial Science and Technology, 1-1-1 Umezono, Tsukuba, Ibaraki, 305-8568, Japan. E-mail: hs.zhou@aist.go.jp; Fax: +81-298-61-5829; Tel: +81-298-61-5795*

***Received (in Montpellier, France) 15th July 2004, Accepted 15th October 2004***
***First published as an Advance Article on the web 17th January 2005***



We have studied the changes in the adsorption characteristics of mesoporous silicate (SBA-15) for benzene and toluene that are caused by using different calcination temperatures ($T_c$ = 773 to 1173 K) in the synthesis process. We found that SBA-15 calcined at 773 K shows an extremely high benzene selectivity, especially in the low pressure region, while SBA-15 treated at higher $T_c$ shows lower selectivity. In order to analyze the benzene selective mechanism, we studied the structures of the SBA-15 series, including their meso- and microporosity in detail. We found that the BET surface area ($S_{BET}$) and the peak position of the mesopore diameter ($2R_p$) decreased, the peak position of the micropore diameter ($2r_p$) increased, and the $2r_p$ distribution became broader with increasing $T_c$. Among above factors, we conclude that the size and the distribution of $2r_p$ are the most important to achieve a high benzene selectivity.

## Introduction

Ordered mesoporous materials have attracted considerable interest because of their great potential for wide-ranging applications in catalysis,[1–3] catalytic supports,[4] sensors,[5] adsorbents,[6] batteries and fuel cells[7] and nanosize patterning.[8] Beck *et al*. have synthesized novel ordered mesoporous silicates by using a commercially obtained triblock copolymer, a star diblock copolymer, and oligomeric surfactants as template agents to obtain several different porous structures.[9] The triblock templatie has advantages for the preparation of periodic porous structured materials with larger pores (2–50 nm), compared with zeolites or ionic surfactant templated mesoporous silicates such as MCM-41, for the incorporation of molecules or functional groups into the pores. These polymer templated ordered silicates were synthesized in various forms: powders,[9,10] thin films,[11–16] fibres,[17] rods,[18] monoliths,[19] spheres,[20,21] and other forms,[22,23] as were ionic surfactant templated mesoporous silicates. Among the ordered mesoporous silicate family, hexagonally ordered SBA-15, which is synthesised by using the triblock copolymer $EO_{20}$-$PO_{70}$-$EO_{20}$ (P123) as a templating agent, is currently the most prominent due to its stability under the synthesis conditions.

The most significant property of mesoporous silicates is their uniform porosity because the utility of porous materials is largely due to the structure and size of their pores. We have developed a microfluidic gas sensor to detect and identify some environmental pollutant gases, namely, benzene, toluene and xylene (BTX), by employing SBA-15 as a gas adsorbent. We succeeded to take advantage of SBA-15 in our sensor because we found that the device response can be controlled by using the structural differences of the pores of the adsorbents.[24]

The pore sizes of porous materials are classified into three categories in the IUPAC definition:[25] micropore (pore diameter ~0.5–2 nm), mesopore (2–50 nm) and macropore (>50 nm). The pore size of the mesopores in SBA-15 has been well-studied by different techniques,[26] while its microporous structure is a subject of current interest.[27–29] Ryoo *et al*. found evidence for the presence of micropores by nitrogen adsorption analysis on some calcined SBA-15 and the connectivity of the ordered mesopores by analysing its inverse platinum replicas.[30] Other studies showed that the mesopore size of SBA-15 depends on the synthesis conditions and calcination temperature. SBA-15 that is synthesised at lower temperatures or calcined at higher temperatures has smaller size mesopores.[31] Galarneau *et al*. reported that when the synthesis temperature of SBA-15 is higher than 80 °C, the mesopore size increases and the wall thickness (that is, the length of the micropore cylinder that connects the mesopore cylinders) decreases. They also reported the collapse of "ultramicroporosity", which they defined as pores that are smaller than 1 nm in diameter.[29] However, the micropore size dependence on the calcination temperature has not yet been studied.

In this paper, we first report the changes in the adsorption characteristics for benzene and toluene of SBA-15 prepared using different calcination temperatures in the synthesis process. We found that one of the SBA-15 samples showed a high benzene selectivity. We successfully explain the benzene selective mechanism by studying the structures of the SBA-15 series, including the meso- and microporosity, in detail.

## Experimental

SBA-15 was prepared as follows using a method almost identical to the previously published technique.[24] We dissolved P123 (BASF Corporation, Pluronic P123, $M_w$ = 5750) in a dilute HCl aqueous solution while stirring it at 313 K. We then added a silica precursor, tetraethyl orthosilicate (TEOS), to the above solution also while stirring it at 313 K. The mole ratio of the chemicals used was 1 TEOS : 0.017 P123 : 5.7 HCl : 193 $H_2O$. We thus obtained a precipitated product that appeared in the solution mixture. We aged the precipitated

DOI: 10.1039/b410851e

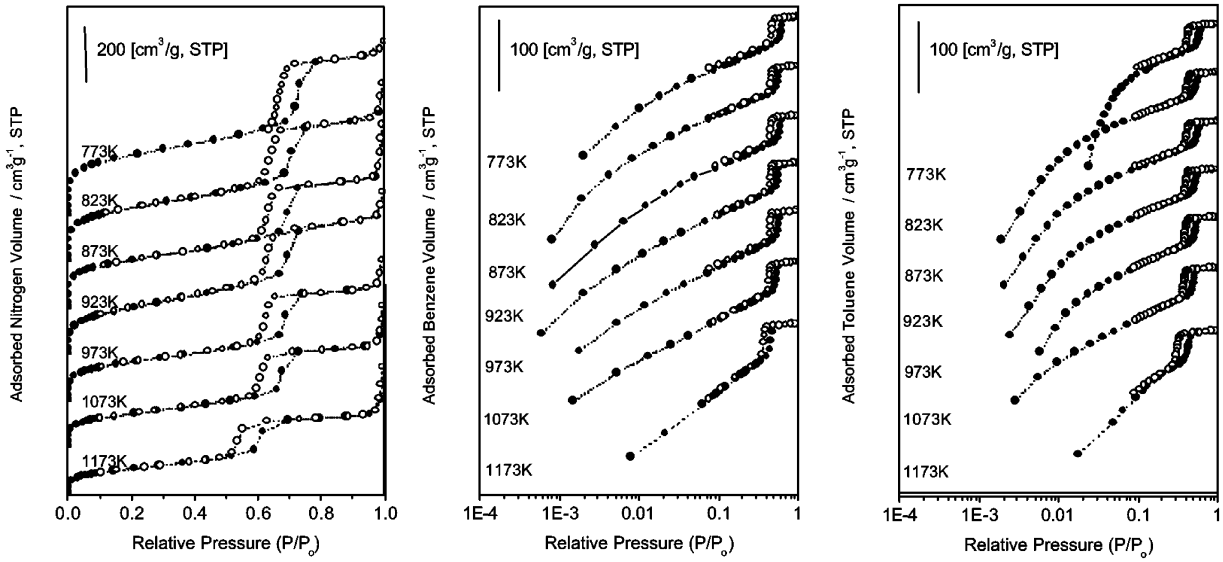


**Fig. 1** Adsorption-desorption isotherms for nitrogen (left), benzene (centre) and toluene (right) of SBA-15-773, SBA-15-823, SBA-15-873, SBA-15-923, SBA-15-973, SBA-15-1073 and SBA-15-1173. Adsorption (filled symbols) and desorption (open symbols) points are overlaid.



product in the solution mixture at 353 K for 1 day, filtered it from the solution, rinsed it with water, and then air-dried it at room temperature. Finally, we calcined the dried, precipitated product by slowly increasing the temperature from room temperature to $T_c$ (773, 823, 873, 923, 973, 1073, 1173 and 1273 K) over a period of 8 h, and then kept it at the chosen $T_c$ for 6 h. After this we decreased the temperature from $T_c$ to 373 K over 8 h, then allowed the product to cool naturally from 373 K to room temperature. Here we denote the obtained sample with $T_c$ as a suffix: that is SBA-15-773, -823, -873, -923, -973, -1073, -1173 and -1273.

We measured benzene, toluene, and nitrogen adsorption-desorption isotherms of each SBA-15 sample by means of a Belsorp plus 18 (BEL Japan, Inc.). We degassed the liquid adsorbates prior to the measurements. We heated each sample for 6 h at 723 K under a pressure of around 10 Pa prior to each measurement. The adsorption-desorption temperature was 293 K (benzene and toluene) or 77 K (nitrogen).

We measured the powder X-ray diffraction (XRD) patterns and the transmittance electron microscope (TEM) images by means of RU-200B (Rigaku Denki) and HF-2000 (Hitachi) operating at 200 keV, respectively. We measured the positron annihilation spectra with a positron annihilation lifetime spectrometer located at AIST, Japan. The positron source and the detector we used were $^{22}$NaCl (about 1.85 MBq) and a plastic scintillator combined with a photomultiplier, respectively. The data were analysed using the maximum entropy lifetime analysis (MELT) computer program.[31–33] We calculated the average of two measurements.

## Results and discussion

### Effect of calcination temperature on benzene and toluene adsorption characteristics

The left panel of Fig. 1 shows nitrogen adsorption-desorption isotherms of SBA-15-773, -823, -923, -973, -1073 and -1173. We note that the results are consistent with the results of Ryoo *et al.*[34,35] We observe type IV physisorption curves that exhibit an H1 type hysteresis loop for all the samples. These hysteresis loops express the particular hysteresis of the capillary condensation due to the mesoporous structure.[36] The shape of the curve is similar for all samples except for SBA-15-1173. The hysteresis is observed at $P/P_o$ ~0.6 to ~0.7 except for SBA-15-1173. This shows that the pore structure may significantly change due to the calcination when $T_c$ is high. We were not able to obtain any reliable results in the nitrogen isothermal measurements of SBA-15-1273 (not shown) because of thermal deterioration of the sample.

The centre and right panels of Fig. 1 show the benzene and toluene adsorption-desorption isotherms of SBA-15-773, -823, -923, -973, -1073 and -1173. The $x$ axis is on a logarithm scale in order to examine the low pressure region in detail. In the $P/P_o > 0.1$ region, both isotherm curves are qualitatively similar to each other. In the results for SBA-15-773, we find that the volume of adsorbed toluene ($V_t$) decreases steeply in the $P/P_o < 0.1$ region while that of benzene ($V_b$) does not. Fig. 2 plots $V_b/V_t$ at $P/P_o$ = 0.03, 0.05 and 0.1. We see that only SBA-15-773 shows a high benzene selectivity, while SBA-15-1173 shows a value larger than 1.0. However, the absolute adsorbed volume is small with this sample and thus the selectivity may be uncertain. The selectivity is larger in the lower pressure region and it drops to 1 when $P/P_o$ is increased to 0.1. This result is consisted with our previous study.[37]

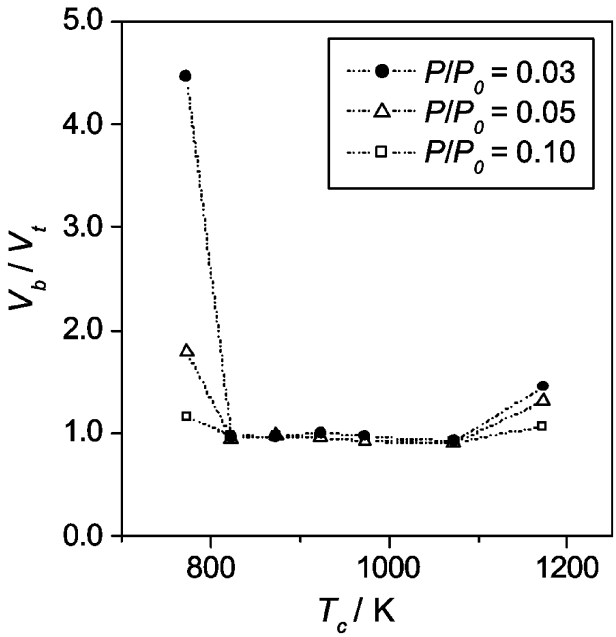


**Fig. 2** $V_b/V_t$ at $P/P_o$ = 0.03 (●), 0.05 (△) and 0.1 (□). We used the values calculated by interpolation by using the measured $V_b$ and $V_t$ around the 0.03 to 0.1 $P/P_o$ region.

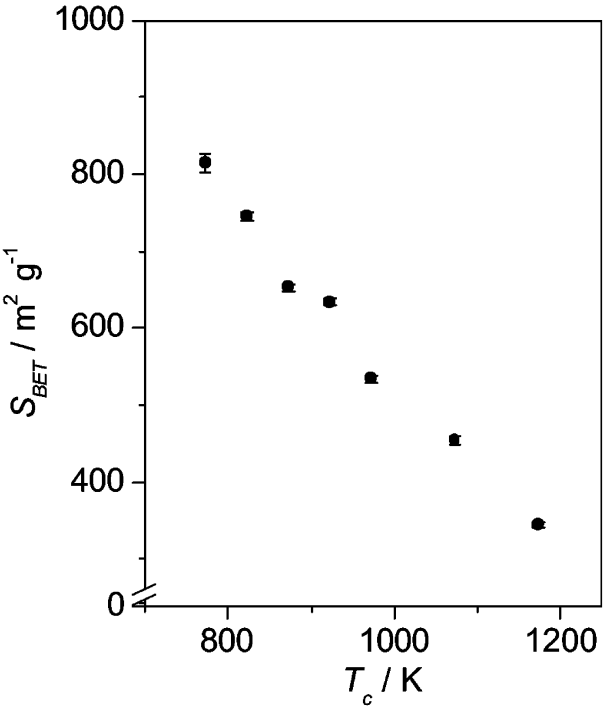


**Fig. 3** $S_{BET}$ dependence on $T_c$ calculated by using the BET method.

However, the difference in adsorbed volumes between benzene and toluene is not significantly large, even in the small $P/P_o$ region, with SBA-15 other than SBA-15-773. This indicates that only SBA-15-773 shows a high benzene selectivity over toluene. In order to analyse the mechanism of the benzene selectivity, we carried out a detailed study of the structure of each SBA-15 sample, including its meso- and microporosities.

### Effect of calcination temperature on meso- and micropore sizes

Fig. 3 plots the specific surface areas ($S_{BET}$) calculated by using the Brunauer–Emmett–Teller (BET) method. We used a value of 0.162 nm$^2$ for the molecular area of nitrogen[38] in the calculations. We repeated the isothermal measurements at least twice on the same sample to confirm the reproducibility of the data. The errors are shown as bars on the plot. We found that $S_{BET}$ decreases with increasing $T_c$. We then studied the porosity change with $T_c$ to describe the changes in $S_{BET}$.

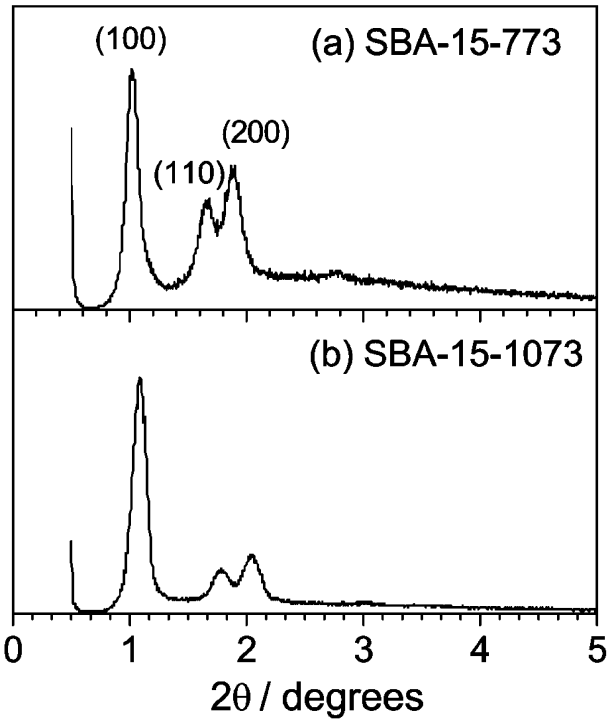


**Fig. 4** XRD patterns of (a) SBA-15-773 and (b) SBA-15-1073.

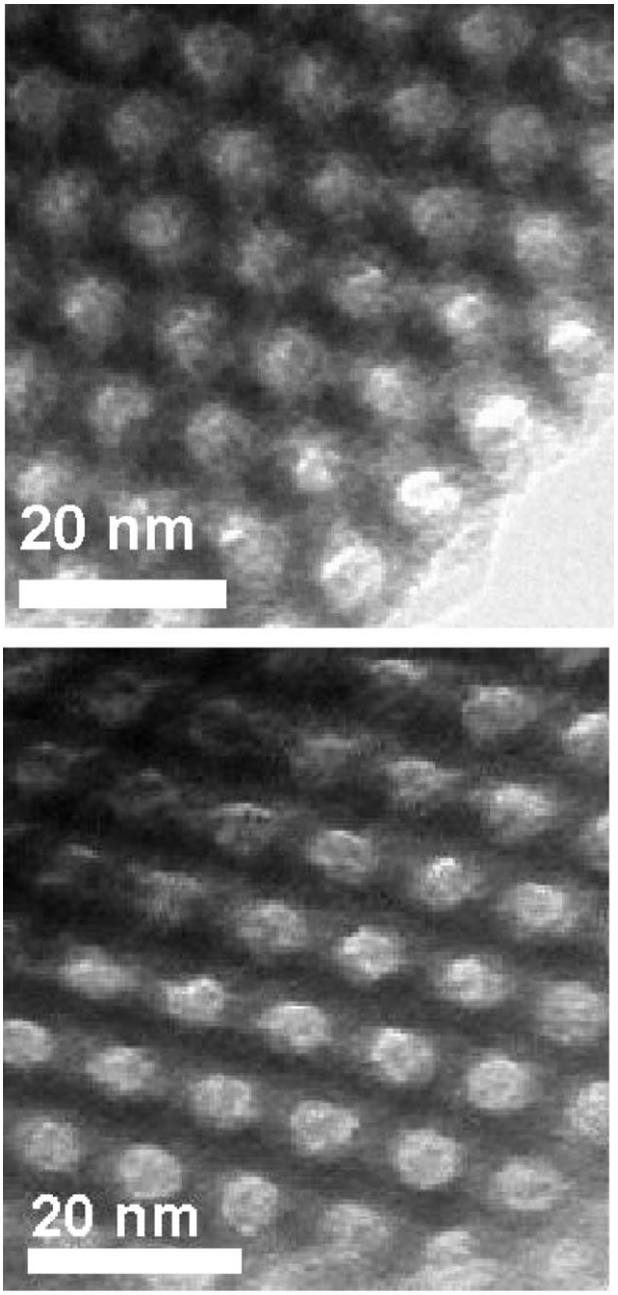


**Fig. 5** TEM images of cross section of SBA-15-773 (upper) and SBA-15-1073 (lower).

Fig. 4 shows the powder XRD patterns of SBA-15-773 and SBA-15-1073. The strongest $2\theta$ peaks are observed at 1.024° and 1.092°; thus, the average distance between the centres of the mesopores ($2L$) was calculated to be 8.6 and 8.1 nm for SBA-15-773 and SBA-15-1073, respectively. The intensity of the peak that corresponds to the (200) reflection is stronger than that of (110). This may be explained by the secondary reflection of (100) falling at a similar angle as that of the (200) peak.

Fig. 5 shows TEM images of SBA-15-773 and SBA-15-1073. Both images clearly show cross sections of the honeycomb-like hexagonal structure of the mesopores of SBA-15. The $2L$ values determined from the Fourier transform of the TEM

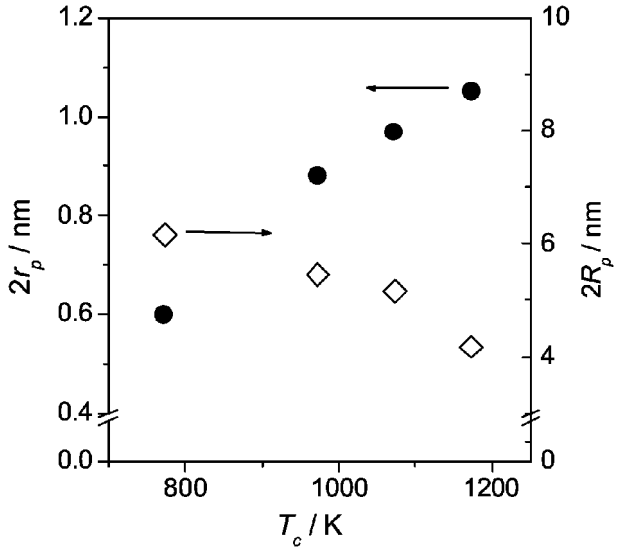


**Fig. 6** $2r_p$ (●, left $y$ axis) and $2R_p$ (◇, right $y$ axis) dependence on $T_c$.

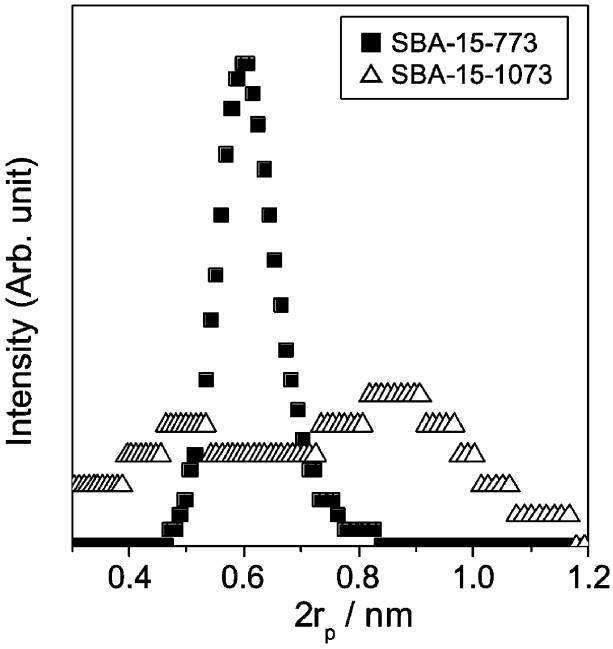


**Fig. 7** $2r_p$ distributions of SBA-15-773 (■) and SBA-15-1073 (△).

images are about 8.2 nm for each sample. However, we have found that electron beam exposure during TEM image measurements can change the pore structure by about $<10\%$ and we thus consider that the $2L$ values calculated from the XRD patterns are more accurate. For the same reason, we cannot discuss the mesopore size difference by using TEM images although the mesopore size of SBA-15-773 is observed to be slightly larger than that of SBA-15-1073.

Fig. 6 plots the $T_c$ dependence of $2R_p$ and $2r_p$ calculated from the nitrogen isotherms by the Dollimore–Heal (DH) method[39] and from positron annihilation spectra, respectively. The standard isotherm was determined for a non-porous sample of $SiO_2$.[39] The peak position of $2R_p$ of SBA-15 decreases with higher $T_c$ (about 6 and 4 nm for SBA-15-773 and -1173, respectively). However, the distribution of $2R_p$ remains as narrow as that of SBA-15-773 ($\pm 0.5$ nm), indicating that the mesopore structure is not destroyed with high $T_c$. This correlates well with what we have observed in the TEM images. In contrast, the peak position of $2r_p$ increases with $T_c$ (about 0.6 and 1.1 nm for SBA-15-773 and -1173, respectively). Moreover, we found that the distribution of $2r_p$ of SBA-15-1073 is much wider than that of SBA-15-773 (Fig. 7). The peak position of $2r_p$ shifts to larger values of the pore size, whereas small size pores are also formed with high $T_c$.

In our previous study, we found that a slight enlargement of the micropores of SBA-15 by an acid treatment leads to significant loss of benzene selectivity.[37] However, this previous result still allows the possibility that the inner surface is changed by the acid treatment, in addition to the size increase. In contrast, as the present experiment does not change the inner surface structure of SBA-15, the small shift of $2r_p$ to larger values or the slight broadening of the $2r_p$ distribution of SBA-15 upon increasing $T_c$ may lead to a significant loss in benzene selectivity. We conclude that the main mechanism for the high benzene selectivity of SBA-15-773 can be explained by its uniform $2r_p$ pore size, which is suitable only for the benzene molecule but not for larger toluene molecule. The benzene selectivity disappears upon enlargement of the micropores with higher $T_c$; the critical $2r_p$ size is about 0.6 nm. These results indicate that fine control of the microporosity is important to achieve control of the gas adsorption properties.

We should also consider that other non-bonding effects such as van der Waals interactions may play a role in discriminating between benzene and toluene.

We can also point out that controlling $T_c$ is a rather simple and useful method to control the pore size of SBA-15. Therefore, we can obtain the desired benzene selective material by careful control of the calcination temperature of SBA-15.

## Conclusion

We found that the selectivity for benzene over toluene can be controlled by carefully choosing the calcination temperature of SBA-15. We studied the structure of a series of SBA-15 samples calcined at different temperatures, including the periodic structure and meso- and microporosities, and found that the peak position of $2R_p$ decreases while that of $2r_p$ increases with higher $T_c$. The distribution of $2R_p$ is not significantly changed by $T_c$ while that of $2r_p$ changes greatly and becomes broader with higher $T_c$. We conclude that the main mechanism for the high benzene selectivity of SBA-15-773 can be explained by its uniform $2r_p$ pore size that is suitable only for the benzene molecule but not for the larger toluene molecule. The critical $2r_p$ value is about 0.6 nm. By precisely controlling the micropore structure, we may obtain ideal porous materials that show an excellent selectivity for certain aromatic hydrocarbon gases. Further studies are required to determine if non-bonding effects such as van der Waals interactions may play a role in discriminating between benzene and toluene.

## References


1 A. Sayari, *Chem. Mater.*, 1996, **8**, 1840.
2 Y. Yue, A. Gedeon, J.-L. Bonardet, N. Melosh, J.-B. D'Espinose and J. Fraissard, *Chem. Commun.*, 1999, 1967.
3 D. T. On, D. Desplanter-Giscard, C. Danumah and S. Kaliaguine, *Appl. Catal., A*, 2003, **253**, 545.
4 V. S.-Y. Lin, D. R. Radu, M.-K. Han, W. Deng, S. Kuroki, B. H. Shanks and M. Pruski, *J. Am. Chem. Soc.*, 2002, **124**, 9040.
5 T. Hyodo, S. Abe, Y. Shimizu and M. Egashira, *Sens. Actuators, B*, 2002, **83**, 209.
6 X. S. Zhao, Q. Ma and G. Q. M. Lu, *Energy Fuels*, 1998, **12**, 1051.
7 X. He and D. Antonellid, *Angew. Chem., Int. Ed.*, 2002, **41**, 215.
8 D. A. Doshi, N. K. Huesing, M. Lu, H. Fan, Y. Lu, K. Simmons-Potter, B. G. Potter, Jr., A. J. Hurd and C. J. Brinker, *Science*, 2000, **290**, 107.
9 C. T. Kresge, M. E. Leonowicz, W. J. Roth, J. C. Vartuli and J. S. Beck, *Nature (London)*, 1992, **359**, 710.
10 J. S. Beck, J. C. Vartuli, W. J. Roth, M. E. Leonowicz, C. T. Kresge, K. D. Schmitt, C. T.-W. Chu, D. H. Olson, E. W. Sheppard, S. B. McCullen, J. B. Higgins and J. L. Schlenkert, *J. Am. Chem. Soc.*, 1992, **114**, 10834.

11 M. Ogawa, *J. Am. Chem. Soc*., 1994, **116**, 7941.
12 M. Ogawa, *Chem. Commun*., 1996, 1149.
13 M. Ogawa, *Langmuir*, 1997, **13**, 1853.
14 M. Ogawa, H. Ishikawa and T. Kikuchi, *J. Mater. Chem*., 1998, **8**, 1783.
15 D. Zhao, P. Yang, N. Melosh, J. Feng, B. F. Chmelka and G. D. Stucky, *Adv. Mater*., 1998, **10**, 1380.
16 T. Yamada, K. Asai, A. Endo, H. S. Zhou and I. Honma, *J. Mater. Sci. Lett*., 2000, **19**, 2167.
17 P. J. Bruinsma, A. Y. Kim, J. Liu and S. Baskaran, *Chem. Mater*., 1997, **9**, 2507.
18 C.-S. Yang, D. D. Awschalom and G. D. Stucky, *Chem. Mater*., 2002, **14**, 1277.
19 N. Melosh, P. Davidson and B. F. Chmelka, *J. Am. Chem. Soc*., 2000, **122**, 823.
20 M. Grün, I. Läuör and K. K. Unger, *Adv. Mater*., 1997, **9**, 254.
21 Q. Huo, J. Feng, F. Schuth and G. D. Stucky, *Chem. Mater*., 1997, **9**, 14.
22 D. Zhao, P. Yang, B. F. Chmelka and G. D. Stucky, *Chem. Mater*., 1999, **11**, 1174.
23 D. Zhao, J. Sun, Q. Li and G. D. Stucky, *Chem. Mater*., 2000, **12**, 275.
24 Y. Ueno, T. Horiuchi, M. Tomita, O. Niwa, H.-S. Zhou, T. Yamada and I. Honma, *Anal. Chem*., 2002, **74**, 5257.
25 *IUPAC Manual of Symbols and Terminology*, Appendix 2, Pt. 1, which appeared in *Pure Appl. Chem*., 1972, **31**, 578.
26 W. W. Lukens, Jr., P. Schmidt-Winkel, D. Zhao, J. Feng and G. D. Stucky, *Langmuir*, 1999, **15**, 5409.
27 K. Miyazawa and S. Inagaki, *Chem. Commun*., 2000, 2121.
28 B. L. Newalkar and S. Komarneri, *Chem. Mater*., 2001, **13**, 4573.
29 A. Galarneau, H. Cambon, F. Di Renzo, R. Ryoo, M. Choi and F. Fajula, *New. J. Chem*., 2003, **27**, 73.
30 R. Ryoo, C. H. Ko, M. Kruk, V. Antochshuk and M. Jaroniec, *J. Phys. Chem. B*, 2000, **104**, 11465.
31 P. Kirkegaard and M. Eldrup, *Comput. Phys. Commun*., 1972, **3**, 240.
32 P. Kirkegaard, M. Eldrup, O. E. Mogensen and N. J. Pedersen, *Comput. Phys. Commun*., 1981, **23**, 307.
33 A. Shukla, M. Peter and L. Hoffmann, *Nucl. Instrum. Methods Phys. Res., Sect. A*, 1993, **335**, 310.
34 H. J. Shin, R. Ryoo, M. Kruk and M. Jaroniec, *Chem. Commun*., 2001, **4**, 349.
35 K. Cassiers, T. Linssen, M. Mathieu, M. Benjelloun, K. Schrijnemakers, P. V. D. Voort, P. Cool and E. F. Vansant, *Chem. Mater*., 2002, **14**, 2317.
36 For example: S. J. Gregg, *Adsorption, Surface Area and Porosity*, Academic Press, New York, 1967, pp. 121–136.
37 Y. Ueno, A. Tate, O. Niwa, H.-S. Zhou, T. Yamada and I. Honma, *Chem. Commun*., 2004, 746.
38 A. L. McClellan and H. F. Harnsberger, *J. Colloid Interface Sci*., 1967, **23**, 577.
39 D. Dollimore and G. R. Heal, *J. Appl. Chem*., 1964, **14**, 109.